

Coarse-Grained Model for Simulation of RNA Three-Dimensional Structures

Zhen Xia,[†] David Paul Gardner,^{‡,§} Robin R. Gutell,^{‡,§} and Pengyu Ren^{*,†,§}

Department of Biomedical Engineering, Section of Integrative Biology and Center for Computational Biology and Bioinformatics, and Institute for Cellular and Molecular Biology, The University of Texas at Austin, Texas 78712, United States

Received: May 28, 2010; Revised Manuscript Received: August 31, 2010

The accurate prediction of an RNA's three-dimensional structure from its "primary structure" will have a tremendous influence on the experimental design and its interpretation and ultimately our understanding of the many functions of RNA. This paper presents a general coarse-grained (CG) potential for modeling RNA 3-D structures. Each nucleotide is represented by five pseudo atoms, two for the backbone (one for the phosphate and another for the sugar) and three for the base to represent base-stacking interactions. The CG potential has been parametrized from statistical analysis of 688 RNA experimental structures. Molecular dynamic simulations of 15 RNA molecules with the length of 12–27 nucleotides have been performed using the CG potential, with performance comparable to that from all-atom simulations. For ~75% of systems tested, simulated annealing led to native-like structures at least once out of multiple repeated runs. Furthermore, with weak distance restraints based on the knowledge of three to five canonical Watson–Crick pairs, all 15 RNAs tested are successfully folded to within 6.5 Å of native structures using the CG potential and simulated annealing. The results reveal that with a limited secondary structure model the current CG potential can reliably predict the 3-D structures for small RNA molecules. We also explored an all-atom force field to construct atomic structures from the CG simulations.

Introduction

The importance of RNA has been appreciated since the central dogma was proposed in 1958.^{1,2} Three RNA molecules, mRNA (mRNA), tRNA (tRNA), and rRNA (rRNA), are associated with the cell's transcription of its DNA into RNA and then translated into proteins.³ While experiments as early as 1971 suggested that RNA is involved in catalysis during protein synthesis,^{4–6} experiments starting in 1982 confirmed that RNA is directly involved in catalysis, in many different RNA systems with difference chemical reactions.^{4,7–15} These RNAs form complex three-dimensional structures.^{16–33}

Within the past few years, a large increase in the number of RNAs that form higher structure, associated with numerous functions in the cell, is the foundation for a major paradigm shift in the molecular biology of the cell; RNAs that do not code for proteins are directly associated with the regulation and overall function of the cell,^{34–44} including different cancers.^{45–47} Since more than 90% of the human genome is transcribed into RNAs that do not code for proteins,^{48,49} and the function of an increasing amount of this RNA is now being determined, the prediction of an RNA higher-order structure and its dynamics will provide great insight into the RNA's contribution to the structure and function of a cell. Toward that end, computational approaches such as molecular modeling have made significant contributions to the understanding of three-dimensional structures and chemical principles of RNA.^{50–60} The most successful approaches for protein structure prediction so far have been

based on comparative analysis or reduced models derived from known structures.^{61–63}

In recent years, increased effort has been devoted to RNA structure prediction as more and more RNA structures have been determined experimentally. A range of models have been developed for nucleic acids, from fully atomistic models to reduced representations.^{64–67} For example, a knowledge-based atomic energy function has been introduced to predict RNA tertiary structures in the FARNAs package.⁶⁸ Nucleotide cyclic motifs are used in MC-Fold and MC-Sym models to build RNA structure from sequence data.⁶⁹ These two models seem successful in predicting the tertiary structure of small RNA molecules. In addition, physics-based atomic force fields such as AMBER^{70–73} and CHARMM^{74–76} describe the dynamic atomic interaction following traditional molecular mechanics, with parameters derived by fitting to ab initio quantum mechanics calculations and experimental data. It is now feasible with supercomputers to simulate dynamic biological systems as large as an entire virus in atomic detail.⁷⁷ However, typical applications of the atomistic force fields are usually limited to small oligomers of nucleic acids or routine simulation times on the order of a few nanoseconds.⁷⁸ On the other hand, coarse-grained (CG) methods reduce the number of particles and eliminate high-frequency motions in the system. A CG model enlarges the time step in molecular dynamics simulations while also enhancing intrinsically faster dynamics.^{79–81} Several CG approaches, either knowledge or physics based, have been utilized to study the structures of nucleic acids.^{68,69,78,82–106}

There has been a history of modeling DNA at meso-scale.^{65,78,82–84,86–89,92–97,99,105} Recently, studies such as Knotts IV and co-workers successfully predicted several important DNA behaviors, like salt-dependent melting, bubble formation, and rehybridization, with a CG model that uses three interaction sites for phosphate, sugar, and base, respectively.⁷⁸ For RNA,

* Corresponding author. Tel.: (512) 232-1832. Fax: (512)-471-0616. E-mail: pren@mail.utexas.edu.

[†] Department of Biomedical Engineering.

[‡] Section of Integrative Biology and Center for Computational Biology and Bioinformatics.

[§] Institute for Cellular and Molecular Biology.

Malhotra et al. first introduced a reduced potential to refine the 3-D structure of low-resolution rRNAs.^{52,59} Zhang et al. combined a highly reduced coarse-grained model and a Monte Carlo method to simulate the distribution of viral RNA inside the capsid of cowpea chlorotic mottle virus.¹⁰⁰ In these works, each nucleotide was modeled as one bead to reduce the complexity of large RNAs. Cao et al. developed a reduced chain representation model to predict RNA folding thermodynamics based on a statistical mechanical theory.¹⁰¹ The RNA molecules were represented by their backbone, and two beads (phosphate and sugar) were used for each nucleotide. Later, Jonikas et al. integrated a coarse-grained model with knowledge-based potentials to generate plausible three-dimensional structures.¹⁰⁷ Despite the development, automated programs for predicting RNA 3-D structures and their dynamic properties are required to increase their accuracy and robustness.¹⁰⁸ In addition, the coarse-grained RNA potentials are mostly aimed at structural refinement rather than predicting dynamics properties.

Aside from the energy or scoring function, the configuration searching and sampling methods are also important components of the structure prediction algorithms. The MC-Fold/MC-Sym and FARNAs programs begin by generating structures from small RNA fragments with a few residues. Then, Las Vegas or Monte Carlo sampling is performed to generate a sampling of possible tertiary structures of the entire RNA.^{68,69} NAST utilizes MD simulations, combined with secondary structure information, to generate 3-D structure candidates for the RNA molecules.¹⁰⁷ A coarse-grained (C3'-based one-bead CG model) energy function derived from the structural statistics is applied in the MD simulation. The ranking of structural clusters can be based on the NAST energy function or experimental data (solvent accessibility data from the hydroxyl radical footprinting).

Herein we present an "intermediate" coarse-grained potential for modeling RNA 3-D structure using molecular dynamics. Previous CG RNA models typically used one^{52,100,107} or two¹⁰¹ particles for each nucleotide. To optimize the efficiency and accuracy, we developed a model that represents each nucleotide with five pseudo atoms: two of these represent the backbone—one for the sugar and the other for the phosphate—while three pseudo atoms represent the stacking and base pairing for each base. The analytical potential energy functional forms, parametrization with 3-D structural statistics obtained from experimental structures and initial validation using molecular dynamics simulations of selected RNAs, are discussed.

Experimental Methods

Data Collection and Preparation. The CG potential was parametrized using statistics collected from available three-dimensional structures of RNA molecules (including both X-ray diffraction structures and nuclear magnetic resonance structures). The RNA structure files were downloaded from The Protein Data Bank (<http://www.pdb.org/>), Nucleic Acid Database (<http://ndbserver.rutgers.edu/index.html>), RNA Comparative Analysis Database (rCAD, <http://rcat.codeplex.com/>, manuscript submitted), and the Comparative RNA Web (CRW) site¹⁰⁹ (<http://www.rna.ccbb.utexas.edu/>). Only 668 structure files that contained more than five base pairs and have the resolution records were analyzed for the statistical calculation. All of the coordinates obtained from nuclear magnetic resonance (NMR) structural files were included in the statistical calculations.

Coarse-Grained RNA Interaction Potential. In our CG model, each nucleotide is reduced to five pseudo atoms in RNA (Figure 1). Two of the five pseudo atoms represent phosphate and sugar, respectively, which is the minimum requirement to

capture the backbone tertiary structures of RNA.¹¹⁰ Each base (A, G, C, and T) is represented by three pseudo atoms, connected by three virtual bonds into a triangle. Compared to earlier models with one particle for each base or each residue,^{78,107} the use of three pseudo atoms for each base provides us with better ability to capture the stacking and pairing of bases. As the different bases share some common pseudo atoms, nine unique types of pseudo atoms are needed to represent the four canonical RNA component bases in total (Figure 1). The improvement in computational efficiency arises from the reduction of number of particles and larger particle mass that enables a greater integration time step in molecular dynamics. The topological and physical properties of the pseudo atoms are listed in Table 1.

The corresponding CG potential energy is calculated by

$$E_{\text{total}} = E_{\text{bonded}} + E_{\text{nonbonded}} \quad (1)$$

where E_{bonded} and $E_{\text{nonbonded}}$ are pairwise bonded and nonbonded energy terms, each representing the sum of contributions of all pairs in the system. The bonded term is further decomposed into

$$E_{\text{bonded}} = E_{\text{bond}} + E_{\text{angle}} + E_{\text{dihedral}} \quad (2)$$

where E_{bond} , E_{angle} , and E_{dihedral} are the bond stretching, angle-bending, and dihedral energies, respectively.

In classical molecular mechanics, the nonbonded interaction consists of the van der Waals (VDW) and electrostatic contributions. Since our CG model is derived from the 3-D structural statistics of experimental structures, an effective potential is used to represent the potential of mean force of all the nonbonded interactions, including the excluded volume repulsive, the attractive force, and the electrostatic force between nonbonded particles, as well as the solvation forces due to the environment. A Buckingham potential is utilized to describe the effective potential (see eq 9).

$$E_{\text{nonbonded}} = E_{\text{effective potential}} \quad (3)$$

For each term, the parametrization was performed based on the Boltzmann inversion of the corresponding atomistic distribution functions obtained from the experimental structures. The Boltzmann inversion method performs a potential inversion from a set of known distributions of structural parameters to extract effective CG potentials. In our RNA CG system, the potentials calculated from the Boltzmann inversion method^{111,112} need to reproduce the distribution of structural parameters including 14 different bonds, 25 types of angles, 28 dihedral angles, and 19 intermolecular radial distribution functions extracted from statistical results of all available atomistic RNA structures (please see Tables 2–5 for more details). All the parameter-fitting works were performed with the software of Matlab Curve Fitting Tool.

Bond Stretching. The distribution of bond lengths can be represented by the Gaussian function, which is calculated by

$$P(l) = \frac{1}{\sqrt{2\pi}\sigma} e^{-(b-l-b_0)^2/2\sigma^2} = e^{-E_{\text{stretch}}/k_B T} \quad (4)$$

where b , b_0 , and σ are the parameters obtained through fitting; k_B is the Boltzmann factor; and T is absolute temperature. Taking

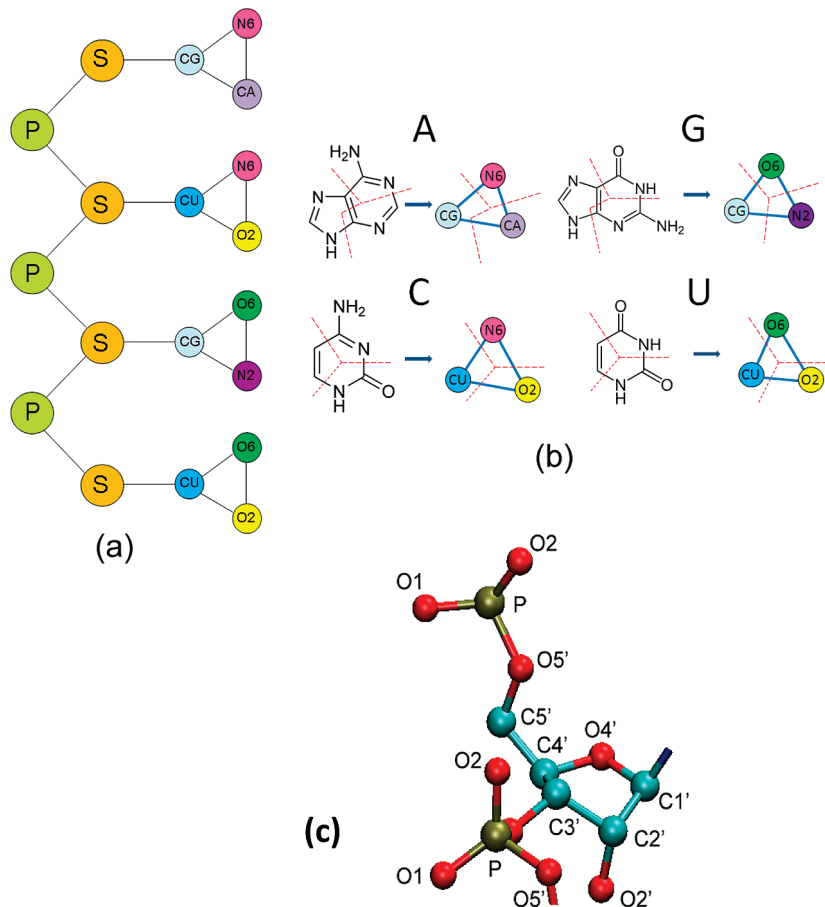


Figure 1. (a) Schematic representation of the CG model for RNA. Phosphate and sugar are represented as one CG particle. The bases A, G, C, and U are represented as three CG particles for each. (b) The components of each CG base. The base is divided by the red dashed line. (c) Schematic representation of all-atom RNA backbone.

TABLE 1: Properties of Nine CG Particles

number	CG particle name	mass (amu)	bond connections
1	P	94.970	2
2	S	97.054	3
3	CG	53.022	3
4	N6	42.030	2
5	N2	54.030	2
6	O6	43.014	2
7	O2	42.006	2
8	CU	26.016	3
9	CA	39.015	2

the logarithm of both sides of eq 4 and dropping the constant term, after performing Boltzmann inversion, we have

$$E_{\text{bond}} = \frac{k_B T}{2\sigma^2} (b - b_0)^2 = K_{\text{bond}} (b - b_0)^2 \quad (5)$$

where the temperature, T , is set to be 298 K.

Angle Bending. The distributions of bond angles can be weighted by a factor $\sin(\theta)$ and renormalized by a factor Z_n . The normalized distribution is expressed as

$$P(\theta) = Z_n p(\theta) / \sin(\theta) = e^{-E_{\text{bend}}/k_B T} \quad (6)$$

where θ is the angle between neighboring bonds, while $P(\theta)$ and $p(\theta)$ are normalized and un-normalized distribution functions of θ . The distributions of bond angles between CG bonds

TABLE 2: Bond Stretching Interaction Parameters for the CG Model of RNA Fitted by the Gaussian Function and Obtained From Statistical Structures

bond	b_0	K_{bond}
1-2	3.85	11.12
2-3	3.74	9.79
2-8	3.61	10.89
3-4	4.29	57.70
3-5	5.66	51.66
3-6	4.28	44.60
3-9	4.33	109.19
4-7	4.55	44.00
4-8	3.59	124.29
4-9	3.53	93.79
5-6	4.57	37.14
6-7	4.53	57.10
6-8	3.55	89.85
7-8	3.52	82.87

were also fitted with the Gaussian function, and then the Boltzmann inversion was used to calculate E_{angle} .

$$E_{\text{angle}} = \frac{k_B T}{2\sigma^2} (\theta - \theta_0)^2 = K_a (\theta - \theta_0)^2 \quad (7)$$

Dihedral Rotation. As in atomic force fields, the torsional energy takes the formula of

TABLE 3: Bond Angle Interaction Parameters for the CG Model of RNA Fitted by the Gaussian Function and Obtained from Statistical Structures

angle	θ_0	K_a
1-2-1	102.78	1.356
1-2-3	101.75	5.271
1-2-3' ^a	75.89	1.864
1-2-8	100.79	9.115
1-2-8'	74.40	2.386
2-1-2	106.18	2.040
2-3-4	154.72	7.130
2-3-5	104.12	12.734
2-3-6	153.94	8.162
2-3-9	108.78	10.611
2-8-4	163.79	6.794
2-8-6	163.79	6.794
2-8-7	88.99	15.930
3-4-9	66.45	35.882
3-5-6	79.38	16.156
3-6-5	48.06	21.701
4-3-9	48.33	49.428
4-7-8	49.44	24.490
4-8-7	79.78	29.398
4-9-3	65.22	17.290
5-3-6	52.57	50.065
6-7-8	50.54	38.613
6-8-7	79.46	31.109
7-4-8	50.84	29.033
7-6-8	49.98	30.600

^a The prime in the table indicates the atom comes from its neighbor residue.

TABLE 4: Optimized CG Parameters for Nonbonded Interaction Described by Equation 9, Including Similar and Unlike Pairs of CG Atoms

CG atoms	σ (initial)	ε (initial) ^a	σ (final)	ε (final) ^b
P-P	11	0.287	11.2778	0.1503
S-S	11.7	0.3827	12.1544	0.4162
C-C	4.4	0.8851	4.1836	0.9276
N6-N6	3.1	1.3875	3.4604	1.4312
N2-N2	4.8	1.1004	4.7928	1.1603
O6-O6	3.1	1.4354	3.7784	1.4635
O2-O2	4.9	1.0526	4.8614	1.0846
C-N6	5.1	0.6698	5.2158	0.3818
O6-O2	5.2	1.0526	5.4321	1.2972
N2-O2	2.8	1.9138	2.7974	2.0524
C-O6	5.2	0.8373	5.26	0.6972
C-O2	3.5	0.909	3.6176	0.8886
N6-O6	2.85	1.866	3.0427	1.8562
C-N2	4.25	0.8373	4.3342	0.8527
N6-O2	5.3	0.7416	5.6477	0.7942
N6-N2	5.3	1.232	5.3832	1.0547
O6-N2	5.4	0.7416	5.5622	0.5273
P-S	9.4	0.5263	9.4287	0.054
S-C	5.6	0.5502	5.615	0.5856

^a Columns σ (initial) and ε (initial) are the nonbonded parameters obtained from statistical potential of mean force. ^b Columns σ (final) and ε (final) are the nonbonded parameters obtained after the optimization.

$$E_{\text{dihedral}}(\phi) = \sum_{n=1}^3 K_n [1 + \cos(n\phi - \delta_n)] \quad (8)$$

where ϕ is the dihedral angle and K_n and δ_n ($n = 1, 2, 3$) are force constants and phase angles. The E_{dihedral} was also obtained from performing Boltzmann inversion.

Nonbonded Interactions. A Buckingham potential,¹¹³ consisting of a 6 term and an exponential term, is used to represent

TABLE 5: Optimized CG Parameters for the Dihedral Interaction Term Described by Equation 8

torsion	V_1	δ_1	V_2	δ_2	V_3	δ_3
1'-2-3-4 ^a	3.354	120	-0.606	180	-0.068	120
1'-2-3-9	3.801	120	0.383	180	-0.287	120
1-2-1'-2'	1.358	0	0.944	180	0.574	0
1-2-3-4	2.964	15	-0.099	180	-0.247	15
1'-2-3-5	3.603	120	1.167	180	-0.325	120
1-2-3-5	3.768	0	0.52	180	0.581	0
1'-2-3-6	3.409	120	-0.265	180	-0.226	120
1-2-3-6	3.077	30	0.306	180	0.246	30
1-2-3-9	3.299	15	0.634	180	-0.204	15
1'-2-8-4	3.461	120	-0.617	180	0.294	120
1-2-8-4	3.321	30	1.121	180	-0.156	30
1'-2-8-6	2.737	120	-0.666	180	0.148	120
1-2-8-6	2.51	30	0.518	180	-0.17	30
1'-2-8-7	3.304	120	1.349	180	-0.342	120
1-2-8-7	3.844	0	0.567	180	0.534	0
2-1-2'-1'	-1.626	135	-0.113	180	-0.246	135
2'-1'-2-3	-1.661	60	0.455	180	0.311	60
2'-1-2-3	1.387	120	0.898	180	-0.516	120
2'-1'-2-8	-1.531	45	0.489	180	0.686	45
2'-1-2-8	1.38	135	0.908	180	-0.691	135
2-3-4-9	7.114	150	-2.4	180	0.516	150
2-3-5-6	-3.328	120	0.95	180	0.101	120
2-3-6-5	5.639	150	-2.063	180	-0.009	150
2-3-9-4	2.959	15	-1.022	180	0.666	15
2-8-4-7	5.024	165	-1.509	180	-1.807	165
2-8-6-7	4.756	165	-1.037	180	-1.455	165
2-8-7-4	-4.072	150	0.544	180	-0.144	150
2-8-7-6	3.51	0	0.425	180	0.457	0

^a The prime in the table indicates the atom comes from its neighbor residue.

the potential of mean force between a pair of nonbonded atoms, i and j

$$E_{\text{nonbonded}} = \varepsilon_{ij} [-2.25(\sigma_{ij}/r_{ij})^6 + 1.84 \times 10^5 e^{-12.00(r_{ij}/\sigma_{ij})}] \quad (9)$$

where ε_{ij} is the depth of the potential well; σ_{ij} is the radius; and r_{ij} is the distance between a pair of atoms. Note that the above equation is used to describe the potential of mean force even though the symbol “ E ” and the formula are commonly used to represent potential energy. The constants we used here are the same as the MM3 force field.^{85,114–116} We use the pair-specific ε and σ parameters instead of the combining rule for unlike atom pair i and j . The Lennard-Jones (LJ) 6-12 potential and Buckingham potential fitted to the nonbonded interactions at the onset were generated. The Buckingham function is “softer” than the LJ 6-12 function in the repulsive region because the exponential term is more suitable to represent the nonbonded potentials in our CG model. However, as shown in Figure S3 (Supporting Information), even the Buckingham potential is not “soft” enough. In addition, some of the interactions (e.g., N2-N2) clearly show a second or more local minima which are ignored by the Buckingham potential. The complicated shape of the nonbonded potentials can be captured much more accurately by using the spline interpolation functions as in the previous statistical potentials for proteins.¹¹⁷ However, in the current study, we would like to explore the capability of the simple Buckingham potential that is implemented in almost all popular molecular modeling packages. In nonbonded potential fitting, we have chosen to primarily reproduce the global energy minima by using a weighted least-squares fit. The data points in the minimum energy area (0.5 Å within the

potential minimum) were assigned a weight of two and the others one. The final fitting results are shown in Figure S3 in the Supporting Information. As discussed in the Results and Discussion section, a nonlinear optimization was later performed on the nonbonded parameters, after all bonded and nonbonded parameters in the CG model were obtained, by minimizing the root-mean-square deviation (rmsd) between the energy-minimized and the experimental structures of selected RNAs. The experimental structures were analyzed to generate the radial distribution functions (RDF) or $g(r)$ for selected pairs of coarse-grained particles (Table 4). The set of 1–2 (directly bonded), 1–3 (separated by two bonds), and 1–4 (separated by three bonds) pairs was not included in RDF calculations. Then the potential of mean force, which corresponds to the Boltzmann inversion of the $g(r)$, is determined from the RDF

$$E_{\text{nonbonded}}(r) = -k_{\text{B}}T \ln g(r) \quad (10)$$

By combining eqs 9 and 10, we determine the initial values of ϵ and σ for each pair. We have also combined certain pairs (the same parameters were used) based on the similarity of the RDF obtained.

Simulation Details. Fifteen different RNA molecules were selected for molecular dynamics simulations using the developed CG potential. For comparison, all-atom simulations were performed on the same set of RNAs using the amber99sb force field with explicit and implicit solvent in AMBER10.^{70,72,118} For the explicit solvent simulations, the TIP3P water model was used.^{119,120} The Particle Mesh Ewald (PME) method^{121,122} was applied to treat the long-range electrostatic interactions, and a 12 Å cutoff was employed for the van der Waals interactions. After the RNA was solved in the water box, 150 mM/L Na⁺ ions were added to the box, and then the Cl[−] ions were added to neutralize the whole system. All the RNA systems were equilibrated with a 5000-step energy minimization to remove the bad contacts. Then, the minimized configurations were used as the starting point for a 1 ns NPT molecular dynamics equilibration at 1 atm and 298 K. For the implicit solvent simulations, the Generalized-Born/Surface Area (GB/SA) model was used.^{123–128} The salt concentration was also 150 mM/L in implicit solvent systems. The time step for all production runs was 1 fs. The CG model molecular dynamics simulations were performed via the modified Beeman algorithm with the TINKER software package.¹²⁹ Different time steps (1 to 10 fs) were tested in the CG MD simulations. The normal simulation time for all systems was 10–100 ns. Simulated annealing MD simulations were performed to fold 15 RNA molecules. In the simulated annealing, after the energy minimization and 2000 steps of equilibrium, the systems were heated to 1000 K within the first 2000 steps and then gradually cooled down to room temperature (298 K) over 100 ns with a linear schedule. For each RNA molecule, we performed five independent simulated annealing simulations starting with random seeds. Finally, we performed another three independent 100 ns simulated annealings under restraints set by the known secondary structure (Watson–Crick base pairs only). A flat-welled harmonic potential (also known as the Nuclear Overhauser Effect potential) was used to restrain the distance between the pseudo atoms CG and AU (Figure 1) in the canonical Watson–Crick base pairs with lower and upper bounds of 8.0 and 10.0 Å, respectively. The force constant for the harmonic potential is zero when the distance falls within the bounds and 0.5 kcal/Å² beyond the bounds.

Results and Discussion

Determination of the RNA Coarse-Grained Model Parameters. The probability distribution of all virtual bonds, angles, and torsions (shown in the Supporting Information) was used to fit the valence parameters using eqs 4–8. The fitted parameters for virtual bonds, angles, and torsions are given in Table 2, Table 3, and Table 5, respectively. The force constants of bonds and angles for pseudo atoms are smaller than those of atomic bonds and angles, meaning a larger time step could be used during the MD simulations in the CG model. As expected, the larger force constants of bonds and angles within the base make the bases fairly stiff (Table 2 and Table 3). However, they are still smaller than those of atomic constants by a factor of 3–10.

The nonbonded parameters in eq 9 were obtained by mapping the radial distribution functions (RDFs) of all the pseudo atoms in existing RNA structures

$$g_{ij}(r) = \frac{1}{N_i d_j} \frac{n_{ij}(r)}{4\pi r^2 \delta r} \quad (11)$$

where $n_{ij}(r)$ is the number of pairs in the given shell from r to $r + dr$; N_i is the total number of particle i in the system; and d is the mean bulk density of particle j . The reference state here is the expected number of contacts when two pseudo atoms i and j are at long distance, which is approximated as the average density of pseudo atoms j .¹³⁰ Therefore, the $g(r)$ could be normalized to 1 at long distance. The results from $g(r)$ are plugged into eq 10 to get the potential of mean force, which is approximated to be the effective potential function of r . The effective potential functions are shown in the Supporting Information. The best fitting results for each type of CG atom are summarized in Table 4.

Optimization of the Nonbonded Parameters. The RNA structural statistics we utilized to derive the nonbonded and bonded parameters effectively include contributions from all energy terms, although to different extents. For example, the actual conformational distribution is affected by both the torsion and nonbonded energy terms in the CG potential. To remove the “redundancy”, we directly compared the structures given by the coarse-grained potential with the experimental structures and adjusted the parameters. Since the RNA structure is most sensitive to the nonbonded interaction, we refined the nonbonded parameters using seven RNA molecules with diverse secondary and tertiary structures. The nonbonded parameters were refined by minimizing the difference between the energy-minimized CG structures and their corresponding experimental structures. First, energy minimization was performed on each of the seven RNA molecules, and the structural rmsd from the experimental structure was calculated based on all pseudo atoms. The average of the rmsd over the seven molecules is used as the target function in the optimization of the nonbonded parameters. An optimally conditioned variable metric nonlinear optimization algorithm in TINKER was utilized.^{129,131–133} The first derivative of the average rmsd with respect to each nonbonded parameter was calculated numerically. In total, 38 nonbonded parameters were optimized (Table 4). The average rmsd between the experimental and energy-minimized structures dropped from 3.35 to 1.75 Å by using the optimized nonbonded parameters.

Validation of the Coarse-Grained Model. We have validated the CG potential in two sets of simulations. First, molecular dynamics simulations of the native RNA structures were performed at room temperature to examine the rmsd

TABLE 6: Comparison of All-Atom Average rmsd's from the Native Crystal Structures for Both the CG Model and the Full-Atom Models^a

PDB ID	rmsd (Å)		
	CG model	full-atom implicit water model (amber99sb ff)	full-atom explicit water model (amber99sb ff)
157D	3.644	5.609	2.260
1DQF	2.478	3.274	1.935
1I9X	3.236	3.956	1.780
2JXQ	2.536	2.940	1.800
2K7E	3.675	4.560	3.560
353D	3.483	2.802	3.583
472D	3.137	2.467	1.500
1F5G	4.425	2.950	1.800
1KD3	4.570	3.740	2.560
1L2X	2.840	2.890	2.730
1LNT	4.751	2.610	1.880
1QCU	1.669	2.560	2.210
1ZIH	3.532	3.180	2.010
2AO5	3.326	2.090	1.350
1AL5	3.080	3.770	2.210
average	3.359	3.293	2.211

^a All rmsd's were obtained from all CG atoms (full-atom calculation using the same atom set as the CG model).

fluctuation. Second, simulated annealing molecular dynamics simulations were applied to fold the RNA structures, with and without restraints set by the secondary structure information. Fifteen RNA molecules with high quality experimental structures were chosen for the model validation (Table 6). These RNAs represent common RNA structural motifs, such as a helix with and without noncanonical base pairs, hairpins, internal loops, bulges, and pseudoknots.

The results of the regular room-temperature MD simulations are given in Table 6. The rmsd's for both the coarse-grained and all-atom model were calculated as an average over the MD trajectories using the same atom set of five pseudo atoms for better comparison. One base pair at each of the terminals is ignored in all the rmsd calculations unless specified otherwise. The 15 RNA molecules investigated had an overall average rmsd with the CG model (3.36 Å). This is similar to the all-atom implicit solvent model (3.30 Å). The all-atom MD simulation with explicit solvent was even closer to the experimental structure, with an average rmsd of 2.21 Å. The rmsd for the CG model (1.66 Å) performed slightly better than the all-atom explicit solvent simulation (2.21 Å) for an A-form helix with canonical Watson–Crick base pairs only. Figure 2a shows the superposition of the native structure (1QCU) and the last frame of 10 ns CG MD simulation. The backbone is well preserved by the CG MD in 1QCU, as well as the base pair and base stacking interactions. As expected, somewhat larger rmsd's have been observed at the 5' and 3' terminals of the double helix in both CG and all-atom MD simulations of 1QCU, consistent with the assumption that the lack of base stacking interactions and neighboring base-pair connections would decrease the stabilities of the helix terminals.

The frameshifting RNA pseudoknot from beet western yellow virus (PDB ID: 1L2X) is a single chain with coaxial helices connected with two loops.¹³⁴ The superposition of the native X-ray structure and the last frame of 10 ns MD CG simulation are shown in Figure 2b. The backbone is well represented in the CG model. The average rmsd of the CG model (2.84 Å) is quite similar to those given by the all-atom simulations using implicit (2.89 Å) and explicit solvent (2.73 Å). Both the all-atom model and the CG model showed a larger fluctuation for

noncanonical Watson–Crick base pairs in 1L2X during the MD simulations. The observed unpaired bases which belong to the loops moved back and forth along the direction perpendicular to the backbone, which may play an important role in forming tertiary contacts.

Among the 15 test RNAs, the largest rmsd (4.75 Å) was observed for 1LNT.¹³⁵ 1LNT is a 24-nt double-strand helix with a 5×5 nt interior loop. The superposition of the native X-ray structure and the final snapshot of MD simulation (Figure 2c) show that the large rmsd is mostly due to the base atoms and two terminals. The bases within the interior loop are much more flexible and disordered than base forming Watson–Crick base pairs. It is not surprising that the current CG model has difficulty in capturing them, given that RNA structures in the parametrization set are dominated by canonical Watson–Crick base pairs.

How well the MD simulations preserve the native structure is only a minimal check of the coarse-grained potential. It is more interesting and challenging to see if the CG potential can be used to “predict” RNA folds. The “folding” of RNA molecules by the CG model was examined by 100 ns simulated annealing molecular dynamics. In this process, the RNA molecule was denatured by being quickly heated to a temperature of 1000 K. With the system temperature gradually (over 100 ns) cooled back down to 298 K, the RNA molecules were expected to fold back to their native or native-like conformations. We have performed five independent simulated annealing runs for each of the 15 RNAs. The final conformations were checked by comparing the structure of the last snapshot of trajectory to its native structure. The minimum and average rmsd's among the five repeats are given in Table 7. The results indicated that ~75% of RNAs fold back to their native-like structures (final all-pseudoatom rmsd < 6.5 Å) at least once among the five repeats. Examples of the simulation snapshots and the final annealed structures of 1ZIH (rmsd = 3.8 Å) and 353D (rmsd = 6.3 Å) could be found at Figure 3b and Figure 3d, respectively. Due to the limited sampling capability of the simulated annealing method, the RNA molecule is very likely to be trapped into a local minimum. For instance, all five simulated annealing repeats of the 1L2X (contains a pseudoknot) failed to fold back to its right coaxial structures and were stuck in different local minima. Another possible reason is a lack of chemical details in our energy potential function. The stability of some RNA tertiary motifs such as pseudoknots is highly dependent on the solvation environment and metal ion concentration, especially the magnesium hydration effect.¹³⁶

Here we discuss in detail three RNAs that were successfully folded by the simulated annealing MD simulations, a hairpin, 1ZIH,^{137,138} and two helices: 353D¹³⁹ and 1DQF.¹⁴⁰ 1ZIH is a 12-nt single strand RAN hairpin capped by a GCAA tetraloop.^{138,141} The GCAA tetraloop belongs to the GNRA tetraloop family (N is A, C, G, or U; R is A or G)¹⁴² which is a basic building block of RNA structure that often provide sites for tertiary contacts or protein binding.^{50,142–145} At the beginning of annealing, the RNA was completely denatured due to the heating, showing a rmsd of about 10 Å (Figure 3a and 3b). The structure became stable after 70 ns, and the rmsd's dropped to ~3.8 Å when the temperature slowly decreased to 400 K (Figure 3b). Similar behavior was observed in the annealing of two A-form helices, 353D (Figure 3d) and 1DQF. 353D contains two U–G Wobbles, and 1DQF contains a bulge residue. Both rmsd's converged to ~4.5 Å at the end of the annealing (Figure 3a). Overall, the successes demonstrate that the CG potential is very promising for ab initio prediction of small RNA tertiary structure from sequence alone.

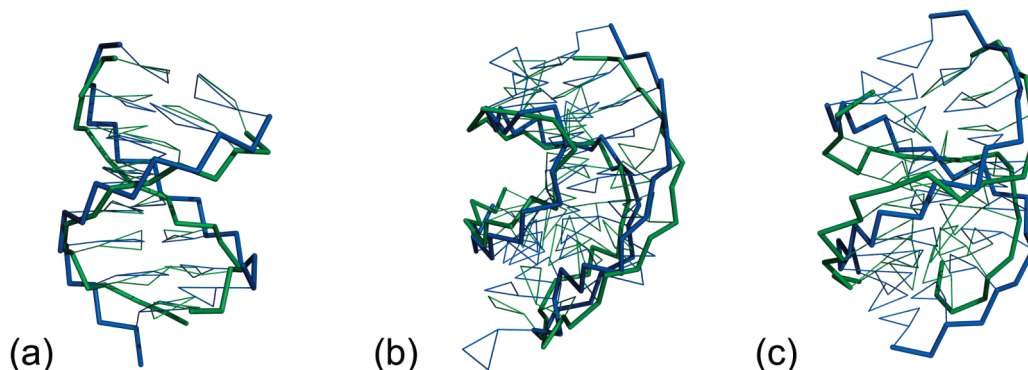


Figure 2. Superposition of the final snapshot from 10 ns CG simulations (colored green) and native structure (colored blue). The backbones are represented as thick sticks, and the bases are shown as lines. (a) Superposition of RNA with 12 canonical Watson–Crick base pairs (PDB ID: 1QCU). (b) Superposition of the frameshifting RNA pseudoknot from beet western yellow virus (PDB ID: 1L2X), a single chain with coaxial helices connected by two loops. (c) Superposition of 24-nt dsRNA with a 5×5 nt internal loop (PDB ID: 1LNT).

TABLE 7: Comparison of All-Atom RMSDs between the Final Structures of 100 ns Simulated-Annealing Simulations to Their Native Structures

PDB ID	rmsd (Å) without restraints	rmsd (Å) with restraints	number of restrained pairs
	MIN/AVG ^a	MIN/AVG	
157D	6.6/7.2	5.2/5.5	5
1AL5	6.4/8.4	5.2/5.8	5
1DQF	4.2/5.7	4.8/5.3	4
1F5G	5.2/7.0	5.8/5.9	5
1I9X	6.8/8.4	3.0/4.7	5
1KD3	8.0/9.1	5.3/5.6	5
1L2X	9.7/10.4	5.0/5.2	5
1LNT	6.5/7.7	5.0/5.6	5
1QCU	6.0/8.8	4.0/4.4	5
1ZIH	3.8/4.7	3.6/5.0	3
2AO5	5.1/6.5	2.8/4.6	5
2JXQ	4.1/6.4	3.0/4.8	5
2K7E	5.9/7.8	5.0/5.1	5
353D	4.8/6.0	4.0/5.5	5
472D	4.6/6.9	4.7/5.5	3

^a The minimum and average rmsd value among all repeats (the restrained pairs shown in the last column on average correspond to ~40% of each RNA).

We have examined the possibility of further refining the CG structures from the simulated annealing by mapping the structures to the corresponding all-atom models and performing all-atom MD simulations. The last frames from the 100 ns simulated annealing simulation of 1ZIH and 353D with rmsd's around 5 Å were taken to generate the initial coordinates for the subsequent all-atom simulations using AMBER10. The all-atom structures were reconstructed from the CG structures via the following steps (please refer to Figure 1c for the atomic labels). (1) The planar all-atom bases were placed based on the three pseudo particles in the CG bases (Figure 1). The C1' atom, which lies in the base plane, was constructed by extending from the N atom in the bases. Equilibrium bond and angle values from the amber99sb force field were used in constructing the atomic coordinates relative to each other. (2) The CG backbone particles P and S were turned into P and C4' in the all-atom model. The backbones O5' and C5' were placed along the vector connecting P and C4' with the P–O5' and O5'–C5' bond lengths to set to be one-third of the P–C4' distance. Similarly, O3' and C3' were placed between C4' and P in the opposite direction. The other two O atoms connecting to P were placed in the plane orthogonal to O3'–P–O4'. (3) The O4' in the sugar ring was placed such that it lied in the plane of C3'–C4'–

O4'–C1'. Using the C4'–O4'–C1' as the anchor, the sugar ring (including directly bonded peripheral atoms) in a flat conformation was then constructed. Note that in this new structure C5' and C3' were moved out of the C4'–P vector. (4) The all-atom structure was then relaxed via AMBER energy minimization, while the five atoms directly transferred from the CG model (three base atoms, P, and C4') were constrained to the CG coordinates. The resulting all-atom structures were subjected to a 20 000-step energy minimization without constraints followed by a 20 ns MD simulation with the amber99sb force field and GB/SA implicit solvation model. For hairpin 1ZIH, the overall rmsd's dropped slightly from ~5.5 to 5 Å. However, the backbone structure of 1ZIH was significantly improved as the rmsd was reduced from 5.4 to 3.65 Å. The detailed base orientations in the GCAA loop could be seen in Figure 3c, which shows the superposition of the final conformation and native structure of the tetraloop. The GCA bases were stacked on top of each other instead of the CAA base stacking in native structure with ~60° rotation. The rotation or flipping of the GNRA bases, similar to the U-turn motif,^{16,33,146} was observed in early studies by NMR analysis and other all-atom molecular dynamic simulations.^{138,147} The flipping of some of the bases toward the solvent in a tetraloop allows those bases to interact with other RNAs and proteins. For 353D, both all-atom rmsd's and backbone rmsd's remained mostly unchanged after the all-atom refinement. One possible reason is that the final structure of CG simulated annealing may be trapped in a local minimum, and the 20 ns all-atom simulation was not able to allow the helix to relax and rearrange into the native structure. The results indicate that the multistage approach is useful for construction and refinement of all-atom structures after the CG simulation provides the prediction of near-native structures.

We also tested the ability of the CG potential to predict 3-D structure when limited restraints are introduced based on the secondary structure information (canonical base pairing) during the simulated annealing simulations. We added restraint by randomly picked 3–5 canonical Watson–Crick base pairs in each RNA molecule (Table 7). With these limited restraints, the CG model was able to predict all the 3-D structures for each tested RNA in all three independent repeats, with rmsd's in the range of 2.8–6.5 Å (Table 7). The results are very encouraging as they demonstrate that limited knowledge of canonical base pairing from secondary structure prediction can greatly facilitate the 3-D structure prediction using a CG potential.

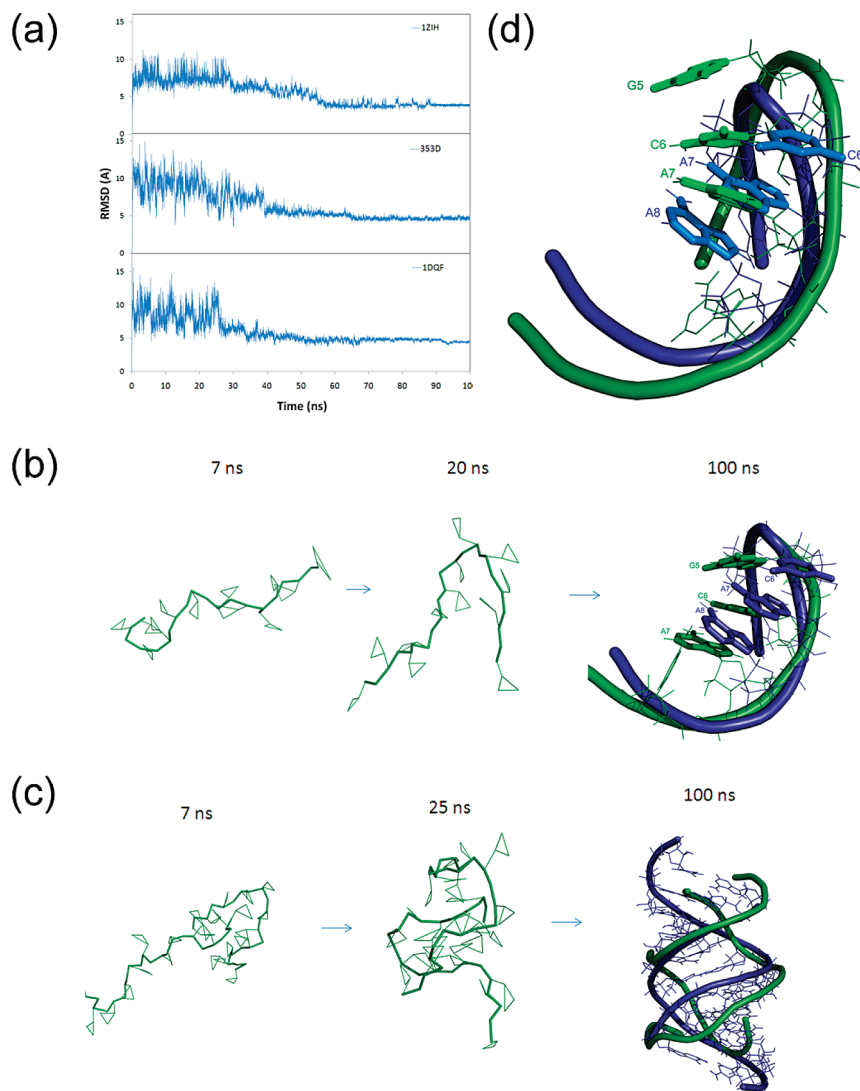


Figure 3. (a) Comparison of all-atom rmsd's for the structures 1ZIH, 353D, and 1DQF during the 100 ns simulated annealing simulations. The simulation temperature was increased to 1000 K within the beginning 2000 steps and then cooled down to room temperature, 298 K. The rmsd's were calculated using all of the CG atoms. The figures show how the RNA molecules fold toward their native structures. (b) Snapshots taken from simulated annealing of 1ZIH. (c) The superposition of the final conformation (colored green) and native structure (colored blue) of the GCCA tetraloop after 20 ns full-atom MD refinement. The backbone is represented as a ribbon, and the base-stacking unit in a tetraloop is shown as sticks. (d) Snapshots taken from simulated annealing simulation of 353D.

Computational Efficiency of the Coarse-Grained Model.

The computational efficiency of the CG model is greatly improved when compared to the all-atom model. A nearly 2 orders of magnitude improvement in MD simulation speed was found with the same time step of 1 fs. This improvement is mainly due to the reduction in the number of bond, angle, and torsion calculations. Furthermore, because of the absence of high-frequency motions such as bond stretching in the all-atom model, a time step up to 10 fs can be applied to the MD simulation without a noticeable effect on energy and structural stability. In addition, in explicit all-atom simulations using a physical force field, not only is the number of atoms further increased due to the presence of the solvent but also the equilibration of water and counterions distribution is time-consuming. Therefore, the CG model can achieve an improvement of about 3 orders of magnitude in the simulation speed, which may enable us to study a large system or extend the simulation time from tens of nanoseconds to the scale of microseconds.

Conclusions

In summary, we developed and applied a new statistical coarse-grained potential to model RNA structures with molecular dynamics. In the coarse-grained potential, each nucleotide is represented by five pseudo atoms including three in the base ring. The bond, angle, torsion, and nonbonded parameters in the CG potential were derived based on the structural statistics sampled from experimental structures of over 600 RNA in PDB. The Boltzmann inversion was used to obtain the initial parameters for the CG potential. Subsequently the nonbonded parameters were optimized analytically by comparing the CG minimum-energy structures with the experimental structures. The optimization was performed systematically using the optimally conditioned variable metric nonlinear optimization algorithm in TINKER.^{129,131–133}

The resulting potential was validated in molecular dynamics simulations of 15 RNAs, including helices, tetraloops, stem loops, bulges, and pseudoknots. Room-temperature MD simulations starting from the native structures produced very reasonable rmsd (3.36 Å on average), indicating the CG potential is able to maintain

the native structure, or the native structures are minima on the CG potential energy surface. The coarse-grained potential was then applied to “predict” the 3-D structures of the 15 RNAs using multiple independent simulated annealing dynamics simulations. For most of the RNAs, at least one out of the five simulated annealing runs, the structure folded into a near native state (rmsd < 6.5 Å). We also noted that the CG potential was able to predict the base stacking behavior in a tetraloop. Furthermore, we also introduced limited distance restraints based on the knowledge of canonical base pairing in the secondary structure. The reliability of the structure prediction using CG potential was drastically improved, and all RNAs were folded into structures with rmsd’s less than 6.5 Å. We also investigated the possibility of using an amber all-atom force field to map and refine the CG model into all-atom structures.

Overall, the performance of this simple CG potential is very promising. With limited knowledge of base-pairing from secondary structure prediction, the CG approach can reliably predict the 3-D structure for small RNA molecules of various topologies. The analytical functional form of the CG potential is compatible with existing molecular modeling packages such as NAMD¹⁴⁸ and GROMACS,¹⁴⁹ so that it can be easily adapted and take advantage of sophisticated simulation algorithms such as the replica exchange molecular dynamic method¹⁵⁰ that is much more effective than simulated annealing for conformational sampling. Further improvement of the accuracy of the CG potential can be achieved by incorporating more experimental structure and refinement of the parameters. To capture the nonbonded interaction more precisely, spline interpolation functions can be utilized instead of the current simple analytical function.¹¹⁷ In the future, extra types of pseudo atoms will be incorporated to represent the modified bases, especially by methylation, such as inosine (derived from adenine) or pseudouridine (derived from uracil) in tRNA.

Acknowledgment. This research is supported by a grant from the Robert A. Welch Foundation to P.R. (F-1691), and R.G. acknowledges support by the Robert A. Welch Foundation (F-1427) and Microsoft Research. Z.X. is grateful to Yue Shi and Dr. Chunli Yan for their help with the AMBER simulations. The authors also acknowledge TeraGrid for providing the computing resources via grant TG-MCB100057.

Note Added after ASAP Publication. This paper was published on the Web on September 30, 2010. An update was made to the Acknowledgment and the corrected version was reposted on October 4, 2010.

Supporting Information Available: The probability distributions of all virtual bonds, angles, and torsions for parametrization are shown in Figures S1, S2, and S4, respectively. The potential of mean force for each coarse-grained pair could be seen in Figure S3. The rmsd’s during 20 ns all-atom simulation refinement are shown in Figure S5. This material is available free of charge via the Internet at <http://pubs.acs.org>.

References and Notes

- (1) Crick, F. *Symp. Soc. Exp. Biol.* **1958**, *XII*, 138.
- (2) Crick, F. *Nature* **1970**, *227*, 561.
- (3) James, D. W.; Tania, A. B.; Stephen, P. B.; Alexander, G.; Michael, L.; Richard, L.; CSHLP, I. *Molecular Biology of the Gene*, 6th ed.; Benjamin Cummings: San Francisco, CA, 2007.
- (4) Stark, B. C.; Kole, R.; Bowman, E. J.; Altman, S. *Proc. Natl. Acad. Sci. U.S.A.* **1978**, *75*, 3717.
- (5) Noller, H. F.; Chaires, J. B. *Proc. Natl. Acad. Sci. U.S.A.* **1972**, *69*, 3115.
- (6) Noller, H. F.; Chang, C.; Thomas, G.; Aldridge, J. *J. Mol. Biol.* **1971**, *61*, 669.
- (7) Kruger, K.; Grabowski, P. J.; Zaug, A. J.; Sands, J.; Gottschling, D. E.; Cech, T. R. *Cell* **1982**, *31*, 147.
- (8) Guerrier-Takada, C.; Gardiner, K.; Marsh, T.; Pace, N.; Altman, S. *Cell* **1983**, *35*, 849.
- (9) Nahvi, A.; Sudarsan, N.; Ebert, M. S.; Zou, X.; Brown, K. L.; Breaker, R. R. *Chem. Biol.* **2002**, *9*, 1043.
- (10) Winkler, W.; Nahvi, A.; Breaker, R. R. *Nature* **2002**, *419*, 952.
- (11) Winkler, W. C.; Cohen-Chalamish, S.; Breaker, R. R. *Proc. Natl. Acad. Sci. U.S.A.* **2002**, *99*, 15908.
- (12) Rodionov, D. A.; Vitreschak, A. G.; Mironov, A. A.; Gelfand, M. S. *Nucleic Acids Res.* **2003**, *31*, 6748.
- (13) Vitreschak, A. G.; Rodionov, D. A.; Mironov, A. A.; Gelfand, M. S. *Trends Genet.* **2004**, *20*, 44.
- (14) Doudna, J. A.; Szostak, J. W. *Nature* **1989**, *339*, 519.
- (15) Noller, H. F.; Hoffarth, V.; Zimniak, L. *Science* **1992**, *256*, 1416.
- (16) Hingerty, B.; Brown, R. S.; Jack, A. *J. Mol. Biol.* **1978**, *124*, 523.
- (17) Ban, N.; Nissen, P.; Hansen, J.; Moore, P. B.; Steitz, T. A. *Science* **2000**, *289*, 905.
- (18) Wimberly, B. T.; Brodersen, D. E.; Clemons, W. M., Jr.; Morgan-Warren, R. J.; Carter, A. P.; Vornrhein, C.; Hartsch, T.; Ramakrishnan, V. *Nature* **2000**, *407*, 327.
- (19) Brodersen, D. E.; Clemons, W. M., Jr.; Carter, A. P.; Wimberly, B. T.; Ramakrishnan, V. *J. Mol. Biol.* **2002**, *316*, 725.
- (20) Kazantsev, A. V.; Krivenko, A. A.; Harrington, D. J.; Holbrook, S. R.; Adams, P. D.; Pace, N. R. *Proc. Natl. Acad. Sci. U.S.A.* **2005**, *102*, 13392.
- (21) Torres-Larios, A.; Swinger, K. K.; Krasilnikov, A. S.; Pan, T.; Mondragon, A. *Nature* **2005**, *437*, 584.
- (22) Serganov, A.; Huang, L.; Patel, D. J. *Nature* **2009**, *458*, 233.
- (23) Cate, J. H.; Gooding, A. R.; Podell, E.; Zhou, K.; Golden, B. L.; Kundrot, C. E.; Cech, T. R.; Doudna, J. A. *Science* **1996**, *273*, 1678.
- (24) Vidovic, I.; Nottrott, S.; Hartmuth, K.; Luhrmann, R.; Ficner, R. *Mol. Cell.* **2000**, *6*, 1331.
- (25) Serganov, A.; Yuan, Y. R.; Pikovskaya, O.; Polonskaia, A.; Malinina, L.; Phan, A. T.; Hobartner, C.; Micura, R.; Breaker, R. R.; Patel, D. J. *Chem. Biol.* **2004**, *11*, 1729.
- (26) Bessho, Y.; Shibata, R.; Sekine, S.; Murayama, K.; Higashijima, K.; Hori-Takemoto, C.; Shirouzu, M.; Kuramitsu, S.; Yokoyama, S. *Proc. Natl. Acad. Sci. U.S.A.* **2007**, *104*, 8293.
- (27) Klein, D. J.; Ferre-D’Amare, A. R. *Science* **2006**, *313*, 1752.
- (28) Serganov, A.; Huang, L.; Patel, D. J. *Nature* **2008**, *455*, 1263.
- (29) Dann, C. E., III; Wakeman, C. A.; Sieling, C. L.; Baker, S. C.; Imov, I.; Winkler, W. C. *Cell* **2007**, *130*, 878.
- (30) Thore, S.; Leibundgut, M.; Ban, N. *Science* **2006**, *312*, 1208.
- (31) Montange, R. K.; Batey, R. T. *Nature* **2006**, *441*, 1172.
- (32) Hainzl, T.; Huang, S.; Sauer-Eriksson, A. E. *Nature* **2002**, *417*, 767.
- (33) Kim, S. H.; Suddath, F. L.; Quigley, G. J.; McPherson, A.; Sussman, J. L.; Wang, A. H.; Seeman, N. C.; Rich, A. *Science* **1974**, *185*, 435.
- (34) Costa, F. F. *Bioessays* **2007**, *32*, 599.
- (35) Spizzo, R.; Nicoloso, M. S.; Croce, C. M.; Calin, G. A. *Cell* **2009**, *137*, 586.
- (36) Frohlich, K. S.; Vogel, J. *Curr. Opin. Microbiol.* **2009**, *12*, 674.
- (37) Georg, J.; Voss, B.; Scholz, I.; Mitschke, J.; Wilde, A.; Hess, W. R. *Mol. Syst. Biol.* **2009**, *5*, 305.
- (38) Khraiweh, B.; Arif, M. A.; Seumel, G. I.; Ossowski, S.; Weigel, D.; Reski, R.; Frank, W. *Cell* **2010**, *140*, 111.
- (39) Hale, C. R.; Zhao, P.; Olson, S.; Duff, M. O.; Graveley, B. R.; Wells, L.; Terns, R. M.; P., T. M. *Cell* **2009**, *139*, 945.
- (40) Marraffini, L. A.; Sontheimer, E. J. *Nat. Rev. Genet.* **2010**, *11*, 181.
- (41) Hamilton, A. J.; Baulcombe, D. C. *Science* **1999**, *286*, 950.
- (42) Lecellier, C. H.; Dunoyer, P.; Arar, K.; Lehmann-Che, J.; Eyquem, S.; Himber, C.; Saib, A.; Voinnet, O. *Science* **2005**, *308*, 557.
- (43) Buchon, N.; Vauray, C. *Heredity* **2006**, *96*, 195.
- (44) Mattick, J. S.; Taft, R. J.; Faulkner, G. J. *Trends Genet.* **2010**, *26*, 21.
- (45) Gupta, R. A.; Shah, N.; Wang, K. C.; Kim, J.; Horlings, H. M.; Wong, D. J.; Tsai, M.-C.; Hung, T.; Argani, P.; Rinn, J. L.; Wang, Y.; Brzoska, P.; Kong, B.; Li, R.; West, R. B.; van de Vijver, M. J.; Sukumar, S.; Chang, H. Y. *Nature* **2010**, *464*, 1071.
- (46) Croce, C. M. *Nat. Rev. Genet.* **2009**, *10*, 704.
- (47) Sassen, S.; Miska, E. A.; Caldas, C. *Virchows Arch.* **2008**, *452*, 1.
- (48) Hahn, M. W.; Wray, G. A. *Evol. Dev.* **2002**, *4*, 73.
- (49) Taft, R. J.; Pheasant, M.; Mattick, J. S. *Bioessays* **2007**, *29*, 288.
- (50) Michel, F.; Westhof, E. *J. Mol. Biol.* **1990**, *216*, 585.
- (51) Levitt, M. *Nature* **1969**, *224*, 759.
- (52) Malhotra, A.; Tan, R. K.; Harvey, S. C. *Biophys. J.* **1994**, *66*, 1777.
- (53) Fink, D. L.; Chen, R. O.; Noller, H. F.; Altman, R. B. *RNA* **1996**, *2*, 851.

- (54) Lehnert, V.; Jaeger, L.; Michel, F.; Westhof, E. *Chem. Biol.* **1996**, *3*, 993.
- (55) Wang, R.; Alexander, R. W.; VanLoock, M.; Vladimirov, S.; Bukhtiyarov, Y.; Harvey, S. C.; Cooperman, B. S. *J. Mol. Biol.* **1999**, *286*, 521.
- (56) Sommer, I.; Brimacombe, R. *J. Comput. Chem.* **2001**, *22*, 407.
- (57) Stagg, S. M.; Mears, J. A.; Harvey, S. C. *J. Mol. Biol.* **2003**, *328*, 49.
- (58) Shapiro, B. A.; Yingling, Y. G.; Kasprzak, W.; Bindewald, E. *Curr. Opin. Struct. Biol.* **2007**, *17*, 157.
- (59) Malhotra, A.; Harvey, S. C. *J. Mol. Biol.* **1994**, *240*, 308.
- (60) Devkota, B.; Petrov, A. S.; Lemieux, S.; Boz, M. B.; Tang, L.; Schneemann, A.; Johnson, J. E.; Harvey, S. C. *Biopolymers* **2009**, *91*, 530.
- (61) Meller, J.; Elber, R. *Comput. Methods Protein Folding* **2002**, *120*, 77.
- (62) Kryshchak, A.; Venclovas, C.; Fidelis, K.; Moulton, J. *Proteins: Struct., Funct., Bioinf.* **2005**, *61*, 225.
- (63) Moulton, J. *Curr. Opin. Struct. Biol.* **2005**, *15*, 285.
- (64) Zwieb, C.; Muller, F. *Nucleic Acids Symp. Ser.* **1997**, *36*, 69.
- (65) Orozco, M.; Perez, A.; Noy, A.; Luque, F. J. *Chem. Soc. Rev.* **2003**, *32*, 350.
- (66) Jossinet, F.; Westhof, E. *Bioinformatics* **2005**, *21*, 3320.
- (67) Wu, J. C.; Gardner, D. P.; Ozer, S.; Gutell, R. R.; Ren, P. *J. Mol. Biol.* **2009**, *391*, 769.
- (68) Das, R.; Baker, D. *Proc. Natl. Acad. Sci. U.S.A.* **2007**, *104*, 14664.
- (69) Parisien, M.; Major, F. *Nature* **2008**, *452*, 51.
- (70) Pearlman, D. A.; Case, D. A.; Caldwell, J. W.; Ross, W. S.; Cheatham, T. E.; Debolt, S.; Ferguson, D.; Seibel, G.; Kollman, P. *Comput. Phys. Commun.* **1995**, *91*, 1.
- (71) Cheatham, T. E., III; Cieplak, P.; Kollman, P. A. *J. Biomol. Struct. Dyn.* **1999**, *16*, 845.
- (72) Case, D. A.; Cheatham, T. E., III; Darden, T.; Gohlke, H.; Luo, R.; Merz, K. M., Jr.; Onufriev, A.; Simmerling, C.; Wang, B.; Woods, R. J. *J. Comput. Chem.* **2005**, *26*, 1668.
- (73) Perez, A.; Marchan, I.; Svozil, D.; Sponer, J.; Cheatham, T. E., III; Laughton, C. A.; Orozco, M. *Biophys. J.* **2007**, *92*, 3817.
- (74) Brooks, B. R.; Brucceeri, R. E.; Olafson, B. D.; States, D. J.; Swaminathan, S.; Karplus, M. *J. Comput. Chem.* **1983**, *4*, 187.
- (75) MacKerell, A. D., Jr.; Banavali, N.; Foloppe, N. *Biopolymers* **2000**, *56*, 257.
- (76) Brooks, B. R.; Brooks, C. L., III; Mackerell, A. D., Jr.; Nilsson, L.; Petrella, R. J.; Roux, B.; Won, Y.; Archontis, G.; Bartels, C.; Boresch, S.; Caffisch, A.; Caves, L.; Cui, Q.; Dinner, A. R.; Feig, M.; Fischer, S.; Gao, J.; Hodoscek, M.; Im, W.; Kuczera, K.; Lazaridis, T.; Ma, J.; Ovchinnikov, V.; Paci, E.; Pastor, R. W.; Post, C. B.; Pu, J. Z.; Schaefer, M.; Tidor, B.; Venable, R. M.; Woodcock, H. L.; Wu, X.; Yang, W.; York, D. M.; Karplus, M. *J. Comput. Chem.* **2009**, *30*, 1545.
- (77) Freddolino, P. L.; Arkhipov, A. S.; Larson, S. B.; McPherson, A.; Schulten, K. *Structure* **2006**, *14*, 437.
- (78) Knotts, T. A.; Rathore, N.; Schwartz, D. C.; de Pablo, J. J. *J. Chem. Phys.* **2007**, *126*, 084901.
- (79) Golubkov, P. A.; Ren, P. Y. *J. Chem. Phys.* **2006**, *125*.
- (80) Scheraga, H. A.; Khalili, M.; Liwo, A. *Annu. Rev. Phys. Chem.* **2007**, *58*, 57.
- (81) Golubkov, P. A.; Wu, J. C.; Ren, P. Y. *Phys. Chem. Chem. Phys.* **2008**, *10*, 2050.
- (82) Maroun, R. C.; Olson, W. K. *Biopolymers* **1988**, *27*, 585.
- (83) Maroun, R. C.; Olson, W. K. *Biopolymers* **1988**, *27*, 561.
- (84) Hao, M. H.; Olson, W. K. *Biopolymers* **1989**, *28*, 873.
- (85) Allinger, N. L.; Yuh, Y. H.; Lii, J.-H. *J. Am. Chem. Soc.* **1989**, *111*, 8851.
- (86) Tan, R. K.; Harvey, S. C. *J. Mol. Biol.* **1989**, *205*, 573.
- (87) Sprou, D.; Harvey, S. C. *Biophys. J.* **1996**, *70*, 1893.
- (88) Sprou, D.; Tan, R. K.; Harvey, S. C. *Biopolymers* **1996**, *39*, 243.
- (89) Tan, R. K.; Sprou, D.; Harvey, S. C. *Biopolymers* **1996**, *39*, 259.
- (90) Massire, C.; Westhof, E. *J. Mol. Graphics Modell.* **1998**, *16*, 197.
- (91) Tanaka, I.; Nakagawa, A.; Hosaka, H.; Wakatsuki, S.; Mueller, F.; Brimacombe, R. *RNA* **1998**, *4*, 542.
- (92) Olson, W. K.; Zhurkin, V. B. *Curr. Opin. Struct. Biol.* **2000**, *10*, 286.
- (93) Matsumoto, A.; Olson, W. K. *Biophys. J.* **2002**, *83*, 22.
- (94) Coleman, B. D.; Olson, W. K.; Swigon, D. *J. Chem. Phys.* **2003**, *118*, 7127.
- (95) Mergell, B.; Ejtehadi, M. R.; Everaers, R. *Phys. Rev. E* **2003**, *68*, 021911.
- (96) Flammini, A.; Maritan, A.; Stasiak, A. *Biophys. J.* **2004**, *87*, 2968.
- (97) LaMarque, J. C.; Le, T. V.; Harvey, S. C. *Biopolymers* **2004**, *73*, 348.
- (98) Nielsen, S. O.; Lopez, C. F.; Srinivas, G.; Klein, M. L. *J. Phys.: Condens. Matter* **2004**, *16*, R481.
- (99) Peyrard, M. *Nonlinearity* **2004**, *17*, R1.
- (100) Zhang, D. Q.; Konecny, R.; Baker, N. A.; McCammon, J. A. *Biopolymers* **2004**, *75*, 325.
- (101) Cao, S.; Chen, S. J. *RNA* **2005**, *11*, 1884.
- (102) Tepper, H. L.; Voth, G. A. *J. Chem. Phys.* **2005**, *122*, 124906.
- (103) Li, X. J.; Kou, D. Z.; Rao, S. L.; Liang, H. J. *J. Chem. Phys.* **2006**, *124*.
- (104) Tan, R. K. Z.; Petrov, A. S.; Harvey, S. C. *J. Chem. Theory Comput.* **2006**, *2*, 529.
- (105) Vologodskii, A. *Biophys. J.* **2006**, *90*, 1594.
- (106) Ding, F.; Sharma, S.; Chalasani, P.; Demidov, V. V.; Broude, N. E.; Dokholyan, N. V. *RNA* **2008**, *14*, 1164.
- (107) Jonikas, M. A.; Radmer, R. J.; Laederach, A.; Das, R.; Pearlman, S.; Herschlag, D.; Altman, R. B. *RNA* **2009**, *15*, 189.
- (108) Ledford, H. *Nature* **2010**, *465*, 16.
- (109) Cannone, J. J.; Subramanian, S.; Schnare, M. N.; Collett, J. R.; D'Souza, L. M.; Du, Y.; Feng, B.; Lin, N.; Madabusi, L. V.; Muller, K. M.; Pande, N.; Shang, Z.; Yu, N.; Gutell, R. R. *BMC Bioinf.* **2002**, *3*, 2.
- (110) Duarte, C. M.; Pyle, A. M. *J. Mol. Biol.* **1998**, *284*, 1465.
- (111) Tschop, W.; Kremer, K.; Batoulis, J.; Burger, T.; Hahn, O. *Acta Polym.* **1998**, *49*, 61.
- (112) Muller-Plathe, F. *ChemPhysChem* **2002**, *3*, 754.
- (113) Buckingham, R. A. *Proc. R. Soc. London, Ser. A* **1938**, *168*, 264.
- (114) Allinger, N. L.; Yuh, Y. H.; Lii, J. H. *J. Am. Chem. Soc.* **1989**, *111*, 8551.
- (115) Lii, J. H.; Allinger, N. L. *J. Am. Chem. Soc.* **1989**, *111*, 8566.
- (116) Lii, J. H.; Allinger, N. L. *J. Am. Chem. Soc.* **1989**, *111*, 8576.
- (117) Summa, C. M.; Levitt, M. *Proc. Natl. Acad. Sci. U.S.A.* **2007**, *104*, 3177.
- (118) Case, D. A.; Darden, T. A.; Cheatham, T. E.; Simmerling, C. L.; Wang, J.; Duke, R. E.; Luo, R.; Crowley, M.; Walker, R. C.; Zhang, W.; Merz, K. M.; Wang, B.; Hayik, S.; Roitberg, A.; Seabra, G.; Kolossvary, I.; Wong, K. F.; Paesani, F.; Vanicek, J.; Wu, X.; Brozell, S. R.; Steinbrecher, T.; Gohlke, H.; Yang, L.; Tan, C.; Mongan, J.; Hornak, V.; Cui, G.; Matthews, D. H.; Seetin, M. G.; Sagui, C.; Babin, V.; Kollman, P. A. *AMBER 10*; University of California, San Francisco, 2008.
- (119) Jorgensen, W. L.; Chandrasekhar, J.; Madura, J.; Impey, R. W.; Klein, M. L. *J. Chem. Phys.* **1983**, *79*, 926.
- (120) Neria, E.; Karplus, M. *J. Chem. Phys.* **1996**, *105*, 10812.
- (121) Deserno, M.; Holm, C. *J. Chem. Phys.* **1998**, *109*, 7678.
- (122) Deserno, M.; Holm, C. *J. Chem. Phys.* **1998**, *109*, 7694.
- (123) Still, W. C.; Tempczyk, A.; Hawley, R. C.; Hendrickson, T. J. *Am. Chem. Soc.* **1990**, *112*, 6127.
- (124) Schaefer, M.; Karplus, M. *J. Phys. Chem.* **1996**, *100*, 1578.
- (125) Scarsi, M.; Apostolakis, J.; Caffisch, A. *J. Phys. Chem. A* **1997**, *101*, 8098.
- (126) Dominy, B. N.; Brooks, C. L. *J. Phys. Chem. B* **1999**, *103*, 3765.
- (127) Bashford, D.; Case, D. A. *Annu. Rev. Phys. Chem.* **2000**, *51*, 129.
- (128) Feig, M.; Im, W.; Brooks, C. L. *J. Chem. Phys.* **2004**, *120*, 903.
- (129) Ponder, J. W. *TINKER - Software Tools for Molecular Design*; Washington University Medical School, 2010.
- (130) Skolnick, J.; Jaroszewski, L.; Kolinski, A.; Godzik, A. *Protein Sci.* **1997**, *6*, 676.
- (131) Shanno, D. F.; Phua, K.-H. *Math. Program.* **1977**, *25*, 507.
- (132) Davidson, W. C. *Math. Program.* **1975**, *9*, 1.
- (133) Shanno, D. F.; Phua, K. H. *J. Optim. Theory Appl.* **1978**, *25*, 507.
- (134) Egli, M.; Minasov, G.; Su, L.; Rich, A. *Proc. Natl. Acad. Sci. U.S.A.* **2002**, *99*, 4302.
- (135) Deng, J.; Xiong, Y.; Pan, B.; Sundaralingam, M. *Acta Crystallogr., Sect. D: Biol. Crystallogr.* **2003**, *59*, 1004.
- (136) Draper, D. E. *Biophys. J.* **2008**, *95*, 5489.
- (137) Heus, H. A.; Pardi, A. *Science* **1991**, *253*, 191.
- (138) Jucker, F. M.; Heus, H. A.; Yip, P. F.; Moors, E. H. M.; Pardi, A. *J. Mol. Biol.* **1996**, *264*, 968.
- (139) Betzel, C.; Lorenz, S.; Furst, J. P.; Bald, R.; Zhang, M.; Schneider, T. R.; Wilson, K. S.; Erdmann, V. A. *Febs. Lett.* **1994**, *351*, 159.
- (140) Xiong, Y.; Sundaralingam, M. *RNA* **2000**, *6*, 1316.
- (141) Correll, C. C.; Swinger, K. *RNA* **2003**, *9*, 355.
- (142) Woese, C. R.; Winker, S.; Gutell, R. R. *Proc. Natl. Acad. Sci. U.S.A.* **1990**, *87*, 8467.
- (143) Doherty, E. A.; Batey, R. T.; Masquida, B.; Doudna, J. A. *Nat. Struct. Biol.* **2001**, *8*, 339.
- (144) Nissen, P.; Ippolito, J. A.; Ban, N.; Moore, P. B.; Steitz, T. A. *Proc. Natl. Acad. Sci. U.S.A.* **2001**, *98*, 4899.
- (145) Cate, J. H.; Gooding, A. R.; Podell, E.; Zhou, K.; Golden, B. L.; Szewczak, A. A.; Kundrot, C. E.; Cech, T. R.; Doudna, J. A. *Science* **1996**, *273*, 1696.
- (146) Jucker, F. M.; Pardi, A. *RNA* **1995**, *1*, 219.
- (147) Sorin, E. J.; Engelhardt, M. A.; Herschlag, D.; Pande, V. S. *J. Mol. Biol.* **2002**, *317*, 493.
- (148) Phillips, J. C.; Braun, R.; Wang, W.; Gumbart, J.; Tajkhorshid, E.; Villa, E.; Chipot, C.; Skeel, R. D.; Kale, L.; Schulten, K. *J. Comput. Chem.* **2005**, *26*, 1781.
- (149) van der Spoel, D.; Lindahl, E.; Hess, B.; van Buuren, A. R.; Apol, E.; Meulenhoff, P. J.; Tieleman, D. P.; Sijbers, A. L. T. M.; Feenstra, K. A.; Drunen, R. v.; Berendsen, C. H. J. www.gromacs.org, (accessed Dec 2005).
- (150) Sugita, Y.; Okamoto, Y. *Chem. Phys. Lett.* **1999**, *314*, 141.